Pharmacophore-guided identification of flavonoid compounds as potential inhibitors for 3C protease of enterovirus A71 and coxsackievirus A16

Thanyada Rungrotmongkol[a,b,*], **Amita Sripattarphan**[a], **Kamonpan Sanachai**[c], **Warinthorn Chavasiri**[d], **Peter Wolschann**[e], **Thierry Langer**[f], **Siwaporn Boonyasuppayakorn**[g,*]

[a] Center of Excellence in Structural and Computational Biology, Department of Biochemistry, Faculty of Science, Chulalongkorn University, Bangkok 10330 Thailand
[b] Program in Bioinformatics and Computational Biology, Graduate School, Chulalongkorn University, Bangkok 10330 Thailand
[c] Department of Biochemistry, Faculty of Science, Khon Kaen University, Khon Kaen 40002 Thailand
[d] Center of Excellence in Natural Products Chemistry, Department of Chemistry, Faculty of Science, Chulalongkorn University, Bangkok 10330 Thailand
[e] Institute of Theoretical Chemistry, University of Vienna, Vienna 1090 Austria
[f] Department of Pharmaceutical Chemistry, Faculty of Life Sciences, University of Vienna, Vienna 1090 Austria
[g] Center of Excellence in Applied Medical Virology, Department of Microbiology, Faculty of Medicine, Chulalongkorn University, Bangkok 10330 Thailand

*Corresponding authors, e-mail: thanyada.r@chula.ac.th, siwaporn.b@chula.ac.th

ABSTRACT: Hand, Foot, and Mouth Disease (HFMD), caused primarily by Enteroviruses A71 (EV-A71) and Coxsackievirus A16 (CV-A16), poses a significant public health concern, particularly in children. The 3C protease (3Cpro) enzymes of these viruses are attractive drug targets for potential antiviral therapies. This study employed computational techniques to identify potential inhibitors for the 3Cpro of EV-A71 and CV-A16. Utilizing rupintrivir as a reference, we developed pharmacophore models and screened a flavonoid database, resulting in the selection of diosmin, epigallocatechin gallate (EGCG), and RTH-011 as promising candidates. Molecular docking studies revealed favorable binding interactions for diosmin and EGCG, suggesting their potential as inhibitors. Experimental validation demonstrated the non-toxic nature of diosmin and EGCG to human Rhabdomyosarcoma (RD) cells and their antiviral activity against EV-A71 and CV-A16. These findings highlight the potential of diosmin and EGCG as promising antiviral agents for HFMD, warranting further drug development efforts.

KEYWORDS: hand foot and mouth disease, coxsackievirus A16, enterovirus A71, EGCG, antiviral inhibitory

INTRODUCTION

Enteroviruses A71 (EV-A71) and coxsackievirus A16 (CV-A16), single-stranded, sense RNA viruses belonging to the *Picornavirales* order's *Enterovirus* genus, are primary pathogens for hand, foot, and mouth disease (HFMD). This disease has spread throughout Asia-Pacific countries, including Australia, Cambodia, China, Japan, Malaysia, Taiwan, Vietnam, and Thailand. The enteroviruses can spread quickly through air via coughing and sneezing of infected individuals. Children under five years are sensitive to HFMD infection. Infected patients have mild fever and rashes on their hands, feet, and mouth [1]. Currently, there are no specific antiviral treatments available for EV-A71 and CV-A16 infections. While supportive care, such as pain relievers and fever reducers, is used to manage symptoms, there is no targeted antiviral therapy or vaccine widely available for these infections, despite ongoing researches in these areas.

A single-stranded sense RNA with a single open reading frame encoding a viral polyprotein precursor is present in both EV-A71 and CV-A16 viruses. The viral polyprotein produced is cleaved by 3C protease (3Cpro) enzyme into four structural (Vp1 to Vp4) and seven nonstructural (2A, 2B, 2C, 3A, 3B, 3C, and 3D) proteins [2]. The 3Cpro (Fig. 1A) is a cysteine protease that favors cleaving peptide bonds between glutamine (Q) and glycine (G) in the viral protein through a reaction involving a catalytic triad (H40, E71, and C147) [3].

The 3Cpro is a prime target for developing anti-HFMD drugs due to its critical function in the life cycles of EV-A71 and CV-A16. The antiviral candidate rupintrivir (AG7088) is a potent peptidomimetic inhibitor of human rhinovirus (HRV) 3Cpro. Additionally, rupintrivir shows broad-spectrum antibiotic activity against other *Picornaviridae* family members, such as CVB2, CVB5, EV6, and EV9 [4–7]. Interestingly, its activity is significantly lower against EV-A71 than HRV [8]. Rupintrivir inhibited EV-A71's 3Cpro with a half-maximal inhibitory concentration of 1.65 μM [2] and Vero cell growth with a half-maximal effective concentration (EC$_{50}$) of 0.78 μM [9].

Flavonoids are natural polyphenolic compounds widely found in plants with various biological func-
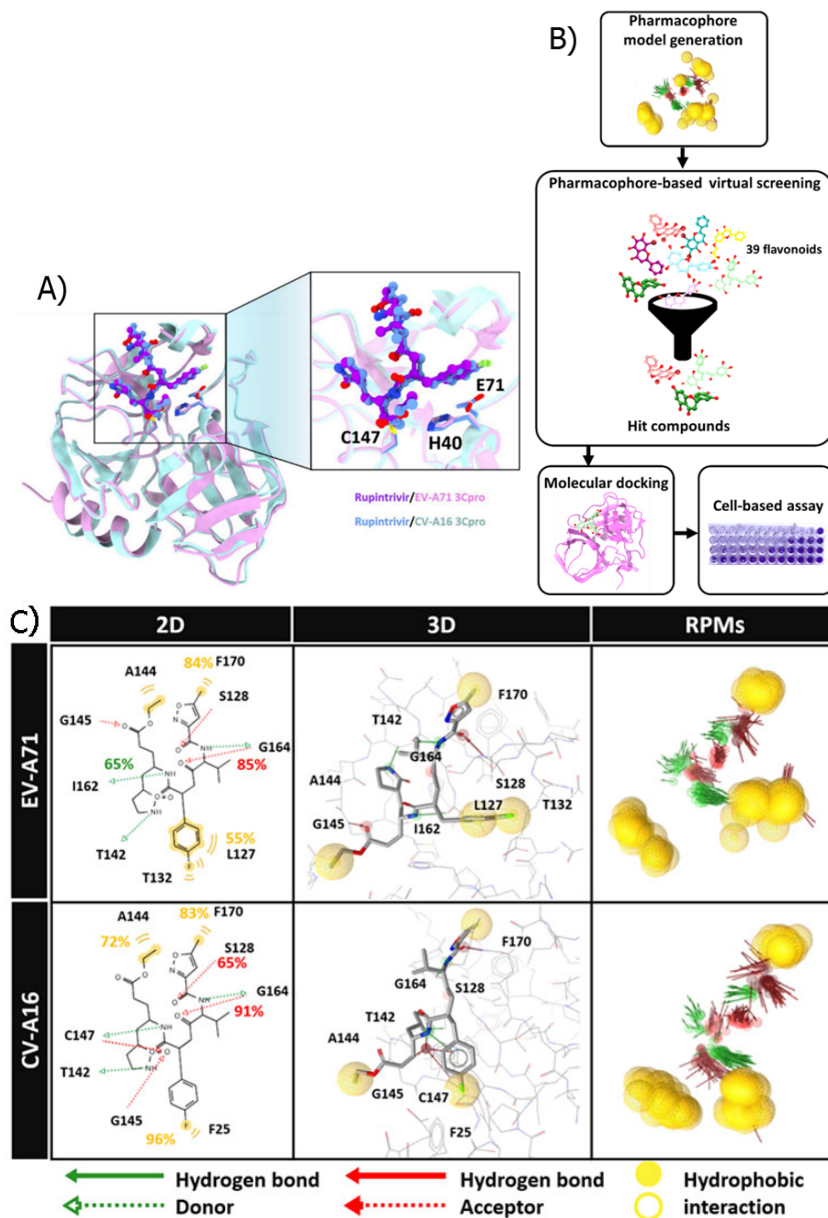
Fig. 1 (A), Superimposed 3Cpro of EV-A71 (PDB ID: 3R0F) and CV-A16 (PDB ID: 3SJI) complexes with rupintrivir (shown in ball-and-stick representation); (B), Workflow for identifying potential compounds against EV-A71 and CV-A16: (i) generating pharmacophore models using simulated EV-A71/rupintrivir and CV-A16/rupintrivir structures, (ii) pharmacophore-based virtual screening of flavonoids, (iii) molecular docking of screened compounds, and (iv) cell-based assay of selected compounds; (C), 2D and 3D pharmacophore models depicting rupintrivir in association with 3Cpro of EV-A71 and CV-A16, alongside interacting residues extracted from the last 50 ns of 500-ns MD simulations [21]. The pharmacophore characteristics are illustrated using green arrows (HBD), red arrows (HBA), and yellow spheres (hydrophobic properties).

tions [10]. They have become compounds of interest for natural drug discovery research. Flavonoids have several pharmacological properties, including antioxidant, anti-inflammatory, anticancer, and antiviral activities [11]. Quercetin demonstrated inhibitory activity against the NS3, a serine protease, of hepatitis C virus (HCV) [12]. Additionally, several flavonoids, including myricetin, astragalin, rutin, epigallocatechin gallate (EGCG), epicatechin gallate, gallocatechin gallate, and luteolin, exhibited more than 40% inhibition of the NS2B-NS3 protease of Zika virus [13]. While NS3, crucial for HCV replication and 3Cpro of EV-A71

and CV-A16, belong to distinct protease families, their shared function in cleaving viral polyproteins has led to the evolution of structural similarities, particularly within their active sites. Despite these similarities, the sequence identity between EV-A71 and CV-A16 remains relatively low at 18.50% and 27.50%, respectively. Although NS3 and 3Cpro have distinct overall folds, they share several structural elements, including alpha-helices and beta-sheets, that contribute to their catalytic function. A key similarity lies in their catalytic triads, essential for proteolytic activity. NS3's catalytic triad consists of H1083 and D1107 in the N-terminal domain and S1165 in the C-terminal domain [14]; while 3Cpro's triad includes H40, E71, and C147. Both enzymes also possess specific substrate binding sites that recognize and cleave viral polyproteins.

A pharmacophore-based screening approach is a highly efficient computational tool for rapidly and accurately sifting through vast databases containing millions of compounds. This method leverages the three-dimensional (3D) interaction patterns, or pharmacophore models, of known drug-like compounds to identify potential candidates that share similar binding characteristics. By focusing on these essential features, researchers can significantly narrow down the search space and prioritize compounds with a higher likelihood of biological activity [2, 10–12]. In the context of drug discovery, pharmacophore modeling can help to identify potential drug candidates, optimize existing drugs, and design new drugs [15]. Several computational techniques have become the most effective drug discovery and development methods. For instance, novel HCV polymerase inhibitors were identified through a pharmacophore-based virtual screening of the Asinex Ltd chemical library, using HCV-796 as a reference inhibitor. Among the 18 hits, compounds 1 and 2 demonstrated inhibitory activities of 54% and 48%, respectively, against HCV polymerase at a concentration of 20 μM [16]. Through pharmacophore modeling, natural product library for potential inhibitors of SARS-CoV-2's main protease (Mpro) were screened [17]. Eight terpenoid compounds emerged as promising candidates. The diterpene nucleus, a common structural feature among these compounds, demonstrated potential as a scaffold for developing novel Mpro inhibitors, underscoring the therapeutic value of natural products in combating COVID-19 [18]. In another study, a pharmacophore model was constructed to identify potential inhibitors for the allosteric site of dengue virus NS5 RNA-dependent RNA polymerase (RdRp). A screening of an approved drug database yielded four promising candidates: desmopressin, rutin, lypressin, and lanreotide [19]. Finally, a pharmacophore model was employed to screen a database of 1437 compounds for potential HIV-1 integrase inhibitors from BindingDB. Molecular dynamics (MD) simulations revealed key structural features es-

sential for inhibition, including a hydrophobic region, a hydrogen bond donor, and a hydrogen bond acceptor. These findings offer valuable insights for designing novel HIV-1 integrase inhibitors [20].

In the present study, we aimed to identify novel potential inhibitors within a set of flavonoids that target the 3Cpro of EV-A71 and CV-A16, using pharmacophore-based virtual screening and subsequent molecular docking techniques. We then evaluated the cytotoxicity and the antiviral efficacy of screened compounds against EV-A71 and CV-A16 infections in human rhabdomyosarcoma (RD) cells, as depicted in the flowchart in Fig. 1B.

MATERIALS AND METHODS

Pharmacophore-based virtual screening

Pharmacophore model generation

A dataset of 7500 frames extracted from the final 50 ns of a simulation involving 3Cpro of CV-A16 and EV-A71 complexed with rupintrivir [21] served as the basis for generating pharmacophore models at the binding site. This process was executed using the LigandScout 4.4.2 program within the KNIME analysis platform [22, 23]. To load information onto complex structures and trajectories, PDB reader and DCD trajectory reader nodes were utilized. The pharmacophore features of rupintrivir in conjunction with 3Cpro of EV-A71 and CV-A16 were created through the "Pharmacophore creator" node within the KNIME program, employing default parameters. Subsequently, a pharmacophore clustering node was developed to cluster the distinct pharmacophore models based on chemical features. These unique pharmacophore models were further organized into Representative Pharmacophore Models (RPMs) using the "Pharmacophore writer" node. These RPMs were then employed as templates for the screening of potential novel inhibitors.

Pharmacophore screening

Our in-house library of 39 flavonoid compounds underwent screening against each RPM using the "get best matching conformation" feature in retrieval mode, and their exclusion volume was assessed utilizing the pharmacophore-fit scoring function [24]. Potent compounds were selected based on their resemblance to the reference drug regarding pharmacophore features. The identified hits were compiled in SDF format and visualized using the Ligand Scout 4.2 program. Compounds that exhibited a superior pharmacophore fit score compared with rupintrivir were prioritized for subsequent investigation.

Validation and comparison of screening results

The accuracy of the screening results was assessed by constructing ROC curves and calculating their cor-

responding AUC values, which served as a method validation metric [25]. Active ligands were selected based on their high pharmacophore fit scores, indicating a strong structural similarity to the known inhibitors. Decoy compounds (inactive ligands), designed to structurally resemble active molecules but lacking inhibitory activity against the enzyme, were sourced from the ZINC database using the Decoy Finder tool [26, 27]. ROC values were computed based on the screening of active and decoy datasets for each individual RPM. Subsequently, these values were graphed and analyzed in terms of sensitivity (true positive rate) and specificity (false positive rate), calculated using the following equations:

$$\text{Sensitivity} = \frac{\text{Selected active ligands}}{\text{All selected ligands}} \quad (1)$$

$$\text{Specificity} = \frac{\text{Discarded inactive ligands}}{\text{All inactive ligands}} \quad (2)$$

Molecular docking

The crystal structures of rupintrivir complexed with 3Cpro of EV-A71 (PDB ID: 3R0F) and CV-A16 (PDB ID: 3SJI) were retrieved from the Protein Data Bank (PDB). The structures of the potent compounds were generated and optimized using the HF/6-31G(d) method within Gaussian09 software [28]. Protonation states of the potent ligands at physiological pH 7.4 were predicted using MarvinSketch 21.20 [29, 30]. To validate the docking system, rupintrivir, the reference ligand, was redocked into the central region of each protein's active site utilizing the GOLD program with a genetic algorithm. A docking sphere with a radius of 15 Å around the docked compound and the GOLD scoring function were employed for 3Cpro of both EV-A71 and CV-A16 systems. One hundred docking poses were generated for each system. Visualization of protein-compound interactions was carried out using UCSF ChimeraX ver. 1.3 and Accelrys Discovery Studio 2.5 (Accelrys Inc.) software.

Antiviral cell-based study

Cells and viruses

Human RD cells (ATCC CCL-136) were cultured in Dulbecco's modified Eagle's medium (DMEM; Gibco, Langley, VA, USA) supplemented with 10% fetal bovine serum (FBS, Sigma-Aldrich, St. Louis, MO, USA), 100 IU/ml penicillin and 100 µg/ml streptomycin (Bio Basic Canada, Toronto, ON, Canada), and 10 mM 4-(2-hydroxyethyl)-1-pperazineethanesulfonic acid (Sigma-Aldrich) at 37 °C under 5% CO_2. EV-A71 05876.1 (BRCR, AB204853.1) and CV-A16 (G10, U05876.1) were courtesy of NIH, Thailand). The RD cell line was propagated in DMEM supplemented with 1% FBS at 37 °C under 5% CO_2.

Cytotoxicity

The RD cells were seeded at 1×10^4 cells per well of a 96-well plate and incubated overnight. Compounds were prepared at 6–10 different concentrations in filter-sterilized DMSO (Merck, Darmstadt, Germany) before being added to the cells. The plates were incubated for 48 h, followed by addition of MTS, 3-(4,5-dimethylthiazol-2-yl)-5-(3-carboxymethoxyphenyl)-2-(4-sulfophenyl)-2H-tetrazolium reagent (Promega, Madison, WI, USA) to the cells, incubation according to the manufacturer's protocol, and analysis by spectrophotometer at $A_{450 \text{ nm}}$. Each compound was tested in triplicate. CC_{50} (half-maximal inhibitory concentration) was calculated by nonlinear regression analysis. Results were reported as mean and standard deviation (SD) of three independent experiments. The final concentration of DMSO in the experiment was 1%, as RD cells showed no toxicity at this DMSO concentration and effectively dissolved the compounds in the medium.

Antiviral efficacy of selected compounds

The RD cells were seeded at 5×10^4 cells per well of a 24-well plate and incubated in a growth medium overnight at 37 °C under 5% CO_2. Cells were infected with EV-A71 and CV-A16 at the multiplicity of infection of 0.1 for 1 h with gentle rocking every 15 min. Cells were washed with phosphate buffer saline and incubated in DMEM supplemented with 1% FBS, 100 IU/ml penicillin, and 100 µg/ml streptomycin. The compounds selected after pharmacophore modeling were prepared in DMSO and added to the virus-infected cells during and after infection. Cells were incubated for 72 h at 37 °C under 5% CO_2 humidified chamber. Supernatants were collected, and viral infectivity was assessed [31]. Cells were fixed and stained with 10% formaldehyde (Carlo Erra, Milano, Italy), 5% isopropanol (Merck, Darmstadt, Germany), and 1% crystal violet (Merck, Darmstadt, Germany) for 1 h. The number of plaque-forming units per ml was determined [31]. Data were plotted, and the EC_{50} (half-maximal effective concentration) values were calculated by nonlinear regression analysis. The results were reported as mean and SD of the three independent experiments. The selectivity index was calculated from the CC_{50} to EC_{50} ratio.

Statistical analysis

Data were presented as mean and standard error of the means (SEM). One-way analyses of variance were used to compare groups, followed by Tukey's test for multiple comparisons. Pairing value differences were assessed using an independent t-test. Mean differences were identified at the confidence level of $p \leqslant 0.05$.

RESULTS AND DISCUSSION

Pharmacophore models and hit compounds for 3Cpro of EV-A71 and CV-A16

Pharmacophores represent essential molecular electronic features for recognizing potent compounds that interact with specific biological targets [32]. In this study, pharmacophore characteristics of rupintrivir were elucidated with 3Cpro of EV-A71 and CV-A16 using 7500 snapshots obtained from our previous MD simulations [21]. The resulting pharmacophore models were aligned and clustered, yielding 100 unique RPMs primarily characterized by hydrophobic properties (depicted as yellow spheres in Fig. 1C), hydrogen bond donors (HBDs, illustrated by green arrows), and hydrogen bond acceptors (HBAs, shown as red arrows). The pharmacophore features associated with rupintrivir in the EV-A71 3Cpro complex included four hydrophobic interactions (with L127, T132, A144, and F170), three HBDs (with T142, I162, and G164), and three HBAs (with S128, G145, and G164). Notably, most pharmacophore features identified for the CV-A16 3Cpro complex resembled those in the EV-A71 3Cpro complex. These included three hydrophobic interactions (with F25, A144, and F170), three HBDs (with T142, C147, and G164), and three HBAs (with G145 and C147, and G164). Interactions occurring with a frequency exceeding 50% were labeled as primary interactions for binding. Furthermore, it was observed that the residues interacting with rupintrivir in both proteins largely corresponded to the key binding residues identified in a previous study [21].

Utilizing the RPMs of each complex as templates, a search was conducted within the in-house database containing 39 flavonoids to identify potential compounds with inhibitory properties against the 3Cpro of EV-A71 and CV-A16. This screening process resulted in the identification of four promising compounds for EV-A71 3Cpro and six for CV-A16 3Cpro (Table S1). Subsequently, compounds exhibiting pharmacophore fit scores comparable to or higher than the known inhibitor rupintrivir when bound to EV-A71 3Cpro (46.8) and CV-A16 3Cpro (46.9) were pinpointed. Specifically, EGCG (47.6 and 47.7), diosmin (47.7 and 47.9), and RTH-011 (47.0 and 47.4) were then selected for further evaluation in subsequent steps.

Screening accuracy assessment

The receiver operating characteristic curve (ROC) and its area under the curve (AUC) were employed to validate the screening accuracy. The evaluation focused on the model's capacity to differentiate between 144 decoys and four active compounds, including the reference ligand, for EV-A71 3Cpro; and 216 decoys and six active compounds for CV-A16 3Cpro, as illustrated in the ROC plots (Fig. 2). An AUC value exceeding 0.50 was indicative of reliable results. The AUC values were as follows: 1.00 (1% coverage of the database), 1.00 (5%), 1.00 (10%), and 0.72 (100%) for EV-A71 3Cpro; and 1.00 (1%), 1.00 (5%), 1.00 (10%), and 0.82 (100%) for CV-A16 3Cpro. It was noted that, the percentage coverage of the database, or coverage calculation in AUC, refered to the percentage of compounds in the database predicted to be active at this threshold. These findings affirmed the model's ability to effectively distinguish true compounds from decoys [33], underscoring the suitability of the hit compounds obtained through pharmacophore-based screening for further development as antiviral drugs.

Comparative docking of screened compounds in 3Cpro of EV-A71 and CV-A16
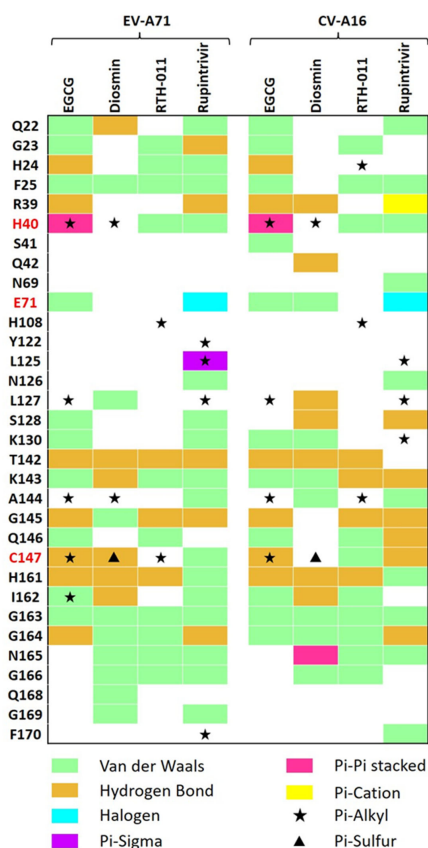
The binding interactions of the screened flavonoids, namely EGCG, diosmin, and RTH-011, with 3Cpro of EV-A71 and CV-A16 were assessed through molecular docking utilizing the GOLD program [34]. As presented in Table S1, diosmin exhibited the highest efficiency among them, with fitness scores of 63.9 and 64.0 for EV-A71 and CV-A16, respectively, followed by EGCG with scores of 60.6 and 60.5, and RTH-011 with scores of 56.2 and 53.9. These docked potent compounds closely aligned with the rupintrivir co-crystal structure at the active site of both viruses [2, 35], as depicted in (Fig. S1). Moreover, they displayed intermolecular interactions with key binding residues similar to those observed for rupintrivir, as illustrated in Fig. 3. In these interactions, van der Waals forces appeared to play a significant role in all flavonoid/3pro complexes. EGCG formed seven hydrogen bonds (with H24, R39, T142, G145, catalytic C147, H161, and G164), five pi-alkyl interactions (with two catalytic residues H40 and C147, as well as L127, A144, and I162), and one pi-pi interaction (with H40) in the case of EGCG/EV-A71. However, in the EGCG/CV-A16 complex, EGCG interacted with S41 instead of S128. Diosmin exhibited fewer interactions with the mentioned residues but compensated with more binding interactions involving N165-G169 in EV-A71; and Q42 and N165-G166 in CV-A16. On the other hand, RTH-011 displayed the fewest interacting residues with both proteins, characterized by 3-4 hydrogen bonds and 2-3 pi-alkyl interactions, which was reflected in its lowest fitness score. The biological activity of these three flavonoids against EV-A71 and CV-A16 was further investigated.

Cytotoxicity and antiviral activity of diosmin and EGCG

The cytotoxicity of diosmin and EGCG was determined through the 3-(4,5-dimethylthiazol-2-yl)-5-(3-carboxymethoxyphenyl)-2-(4-sulfophenyl)-2H-tetrazolium (MTS) assay. While diosmin and EGCG readily dissolved in dimethyl sulfoxide (DMSO), RTH-011 exhibited insolubility in DMSO, leading to its exclusion from further investigation. Both diosmin
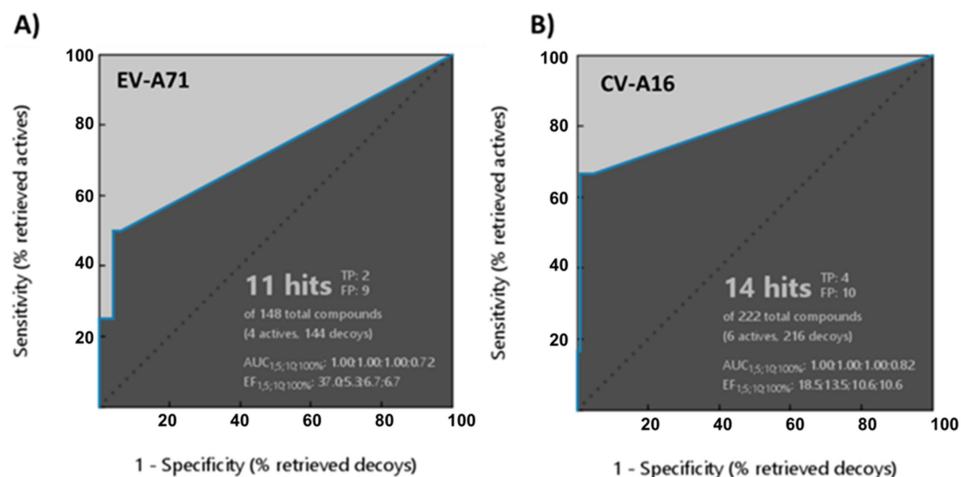
Fig. 2 Receiver operating characteristic (ROC) curves depicting the pharmacophore models performance of: (A), EV-A71 3Cpro; and (B), CV-A16 3Cpro; with AUC values presented for database coverage at 1%, 5%, 10%, and 100%.

Fig. 3 Comparison of intermolecular interactions between the screened flavonoids and rupintrivir with 3Cpro of EV-A71 and CV-A16. The residues with black labels are substrate-binding residues, while those with red labels are catalytic triad residues.

and EGCG demonstrated non-toxicity towards human RD cells, with calculated CC_{50} values exceeding 100 μM for EGCG and over 500 μM for diosmin (Fig. 4). This finding aligned with prior research results, indicating that flavonoids such as chrysin and quercetin exhibited no cytotoxic effects on RD cells at concentrations of 200 μM [36, 37].

The viral inhibition was performed by infecting RD cells with EV-A71 and CV-A16 at the M.O.I. of 0.1. Diosmin and EGCG were prepared at various concentrations. Infected RD cells were washed and replaced with the maintenance medium, diosmin, and EGCG at their respective concentrations. Cells were then incubated for 72 h, and supernatants were collected for plaque titration. The EC_{50} values were determined via nonlinear regression analysis, as shown in Fig. 5. Diosmin exhibited EC_{50} values of 21.02 ± 1.57 μM for EV-A71 and 30.68 ± 3.25 μM for CV-A16, whereas EGCG demonstrated EC_{50} values of 12.86 ± 1.30 μM for EV-A71 and 15.54 ± 1.50 μM for CV-A16. These results indicated the capability of both compounds to reduce the viral titer of EV-A71 and CV-A16. Furthermore, the EC_{50} values of diosmin and EGCG aligned with and resembled the values of various flavonoid compounds previously reported on EV-A71, including chrysin (EC_{50} of 15.89 μM [38]), apigenin (10.3 μM [39]), and quercetin (12.1 μM [40]). Moreover, antiviral activity of EGCG against influenza A (EC_{50} of 22–28 μM [41]), porcine epidemic diarrhea virus (12.39 μM [42]), and Zika virus (21.4 μM [43]) were also highlighted. In addition, both compounds exhibited similar selective indices (Table S2). These findings suggested that diosmin and EGCG might possess antiviral activity against EV-A71 and CV-A16 infections, with notably lower EC_{50} values observed for EV-A71 than CV-A16.

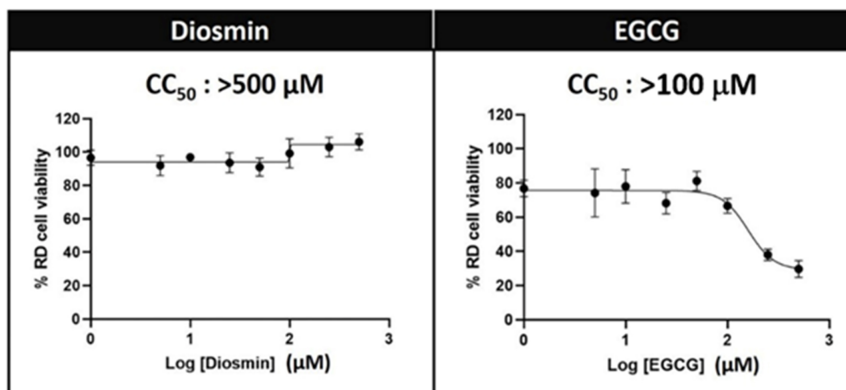Diosmin and EGCG are flavonoids known for their

Fig. 4 Cytotoxicity against RD cells of diosmin and EGCG. The compounds were dissolved and diluted to various concentrations before adding to the RD cells. Cells were incubated for 48 h before the analysis with MTS assay. Three independent experiments were performed to confirm the finding.
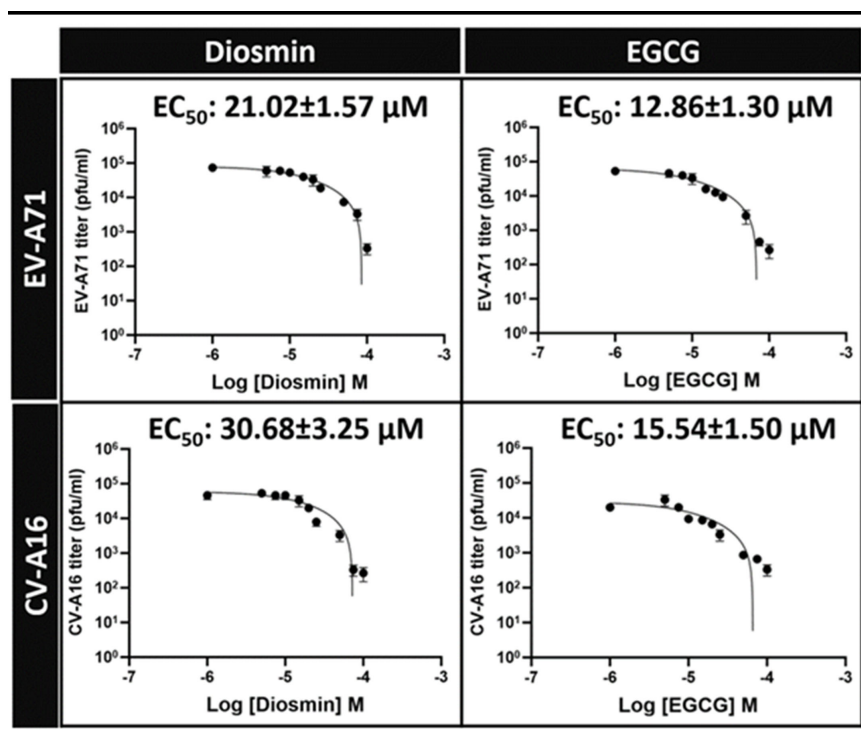

Fig. 5 Inhibitory activity of diosmin and EGCG in RD cells infected with EV-A71 and CV-A16. Effective concentrations were derived from non-linear regression analysis and errors indicated the standard error of the means (SEM) of three independent experiments.

antioxidant and anti-inflammatory properties [44, 45]. While their antiviral potential against HFMD has been investigated, further studies are needed to fully understand their effectiveness. Diosmin, an approved medication, offers a proven safety and efficacy profile. Its antiviral activity against HFMD suggests potential repurposing, although rigorous evaluation of dosage, administration, and potential side effects is essential. If found effective, over-the-counter availability of diosmin or EGCG could improve public accessibility. Public preventive measures, especially for high-risk populations, might benefit from these compounds, but their efficacy requires robust clinical trials. Additional studies, including animal models, are necessary for the investigation of antiviral effects of diosmin and EGCG on HFMD. Well-designed clinical trials are crucial for evaluating their safety, efficacy, and optimal dosage. Exploring combinations with other antiviral agents or

immune modulators could potentially enhance existing therapeutic benefits. Comprehensive research will clarify the antiviral potential of diosmin and EGCG, paving the way for their potential application in HFMD prevention and treatment.

CONCLUSION

This study comprehensively explored pharmacophore models and potential inhibitors for the 3Cpro of EV-A71 and CV-A16. By analyzing MD trajectories of rupintrivir, we elucidated its pharmacophore characteristics, leading to the generation of 100 unique RPMs. These RPMs, characterized by hydrophobic features and hydrogen bond interactions, facilitated the screening of a 39-flavonoid database. Four promising compounds for EV-A71 3Cpro and six for CV-A16 3Cpro were identified, with diosmin, EGCG, and RTH-011 exhibiting higher pharmacophore fit scores than rupintrivir. Molecular docking analysis revealed diosmin as the most potent compound, followed closely by EGCG. The accuracy of our screening process was validated using ROC curves and AUC values, demonstrating its ability to distinguish true compounds from decoys. The identified hit compounds showed potential as antiviral drugs, as evidenced by their binding interactions with key residues in the 3Cpro of EV-A71 and CV-A16 co-crystal structures. Cellular toxicity assessments confirmed the non-toxicity of diosmin and EGCG to human RD cells. Moreover, these compounds exhibited antiviral activity against EV-A71 and CV-A16, as demonstrated by their EC_{50} values. Our findings suggested that diosmin and EGCG could promisingly be potential antiviral agents for EV-A71 and CV-A16, offering potential avenues for the development of HFMD therapeutics.

Appendix A. Supplementary data

Supplementary data associated with this article can be found at https://dx.doi.org/10.2306/scienceasia1513-1874.2025.018.

REFERENCES

1. Cox B, Levent F (2018) Hand, foot, and mouth disease. *Jama* **320**, 2492.
2. Lu G, Qi J, Chen Z, Xu X, Gao F, Lin D, Qian W, Liu H, et al (2011) Enterovirus 71 and coxsackievirus A16 3C proteases: binding to rupintrivir and their substrates and anti-hand, foot, and mouth disease virus drug design. *J Virol* **85**, 10319–10331.
3. Zhang X, Song Z, Qin B, Zhang X, Chen L, Hu Y, Yuan Z (2013) Rupintrivir is a promising candidate for treating severe cases of enterovirus-71 infection: evaluation of antiviral efficacy in a murine infection model. *Antiviral Res* **97**, 264–269.
4. Binford SL, Maldonado F, Brothers MA, Weady PT, Zalman LS, Meador JW 3rd, Matthews DA, Patick AK (2005) Conservation of amino acids in human rhinovirus 3C protease correlates with broad-spectrum antiviral activity of rupintrivir, a novel human rhinovirus 3C protease inhibitor. *Antimicrob Agents Chemother* **49**, 619–626.
5. Binford SL, Weady PT, Maldonado F, Brothers MA, Matthews DA, Patick AK (2007) *In vitro* resistance study of rupintrivir, a novel inhibitor of human rhinovirus 3C protease. *Antimicrob Agents Chemother* **51**, 4366–4373.
6. Ooi MH, Wong SC, Lewthwaite P, Cardosa MJ, Solomon T (2010) Clinical features, diagnosis, and management of enterovirus 71. *Lancet Neurol* **9**, 1097–1105.
7. Patick AK, Binford SL, Brothers MA, Jackson RL, Ford CE, Diem MD, Maldonado F, Dragovich PS, et al (1999) *In vitro* antiviral activity of AG7088, a potent inhibitor of human rhinovirus 3C protease. *Antimicrob Agents Chemother* **43**, 2444–2450.
8. Lu G, Qi J, Chen Z, Xu X, Gao F, Lin D, Qian W, Liu H, et al (2011) Enterovirus 71 and coxsackievirus A16 3C proteases: Binding to rupintrivir and their substrates and anti-hand, foot, and mouth disease virus drug design. *J Virol* **85**, 10319–10331.
9. Tsai M-T, Cheng Y-H, Liu Y-N, Liao N-C, Lu W-W, Kung S-H (2009) Real-time monitoring of human enterovirus (HEV)-infected cells and anti-HEV 3C protease potency by fluorescence resonance energy transfer. *Antimicrob Agents Chemother* **53**, 748–755.
10. Samanta ASD (2011) Roles of flavonoids in plants. *Int J Pharm Sci Tech* **6**, 12–35.
11. Panche AN, Diwan AD, Chandra SR (2016) Flavonoids: an overview. *J Nutr Sci* **5**, e47.
12. Bachmetov L, Gal-Tanamy M, Shapira A, Vorobeychik M, Giterman-Galam T, Sathiyamoorthy P, Golan-Goldhirsh A, Benhar I, et al (2012) Suppression of hepatitis C virus by the flavonoid quercetin is mediated by inhibition of NS3 protease activity. *J Viral Hepat* **19**, e81–88.
13. Lu N, Khachatoorian R, French SW (2012) Quercetin: bioflavonoids as part of interferon-free hepatitis C therapy? *Expert Rev Anti Infect Ther* **10**, 619–621.
14. Kim JL, Morgenstern KA, Lin C, Fox T, Dwyer MD, Landro JA, Chambers SP, Markland W, et al (1996) Crystal structure of the hepatitis C virus NS3 protease domain complexed with a synthetic NS4A cofactor peptide. *Cell* **87**, 343–355.
15. Giordano D, Biancaniello C, Argenio MA, Facchiano A (2022) Drug design by pharmacophore and virtual screening approach. *Pharmaceuticals* **15**, 646.
16. Kim ND, Chun H, Park SJ, Yang JW, Kim JW, Ahn SK (2011) Discovery of novel HCV polymerase inhibitors using pharmacophore-based virtual screening. *Bioorg Med Chem Lett* **21**, 3329–3334.
17. Sanachai K, Wilasluck P, Deetanya P, Wangkanont K, Rungrotmongkol T, Hannongbua S (2023) Targeting the main protease for COVID-19 treatment: A comprehensive review of computational screening and experimen-

tal studies. *ScienceAsia* **49**, 477–484.

18. Wang J, Jiang Y, Wu Y, Yu H, Wang Z, Ma Y (2022) Pharmacophore-based virtual screening of potential SARS-CoV-2 main protease inhibitors from library of natural products. *Nat Prod Commun* **17**, 1–7.

19. Kumar S, Bajrai L, Faizo A, Khateb A, Alkhaldy A, Rana R, Azhar E, Dwivedi V (2022) Pharmacophore-model-based drug repurposing for the identification of the potential inhibitors targeting the allosteric site in dengue virus NS5 RNA-dependent RNA polymerase. *Viruses* **14**, 1827.

20. Islam MA, Pillay TS (2016) Structural requirements for potential HIV-integrase inhibitors identified using pharmacophore-based virtual screening and molecular dynamics studies. *Mol BioSys* **12**, 982–993.

21. Sripattaraphan A, Sanachai K, Chavasiri W, Boonya-suppayakorn S, Maitarad P, Rungrotmongkol T (2022) Computational screening of newly designed compounds against coxsackievirus A16 and enterovirus A71. *Molecules (Basel, Switzerland)* **27**, 1908.

22. Beisken S, Meinl T, Wiswedel B, de Figueiredo LF, Berthold M, Steinbeck C (2013) KNIME-CDK: Workflow-driven cheminformatics. *BMC Bioinformatics* **14**, 257.

23. Wolber G, Langer T (2005) LigandScout: 3-D pharmacophores derived from protein-bound ligands and their use as virtual screening filters. *J Chem Inf Model* **45**, 160–169.

24. Hengphasatporn K, Garon A, Wolschann P, Langer T, Yasuteru S, Huynh TNT, Chavasiri W, Saelee T, et al (2020) Multiple virtual screening strategies for the discovery of novel compounds active against dengue virus: A hit identification study. *Sci Pharm* **88**, 2.

25. Fawcett T (2006) An introduction to ROC analysis. *Pattern Recognit Lett* **27**, 861–874.

26. Mysinger MM, Carchia M, Irwin JJ, Shoichet BK (2012) Directory of useful decoys, enhanced (DUD-E): Better ligands and decoys for better benchmarking. *J Med Chem* **55**, 6582–6594.

27. Adriá CM, Garcia-Vallvé S, Pujadas G (2012) DecoyFinder, a tool for finding decoy molecules. *J Cheminform* **4**(Suppl 1), P2.

28. Frisch MJ (2009) Gaussian09.

29. ChemAxon (2018) MarvinSketch.

30. Yepes-Pérez AF, Herrera-Calderon O, Sánchez-Aparicio JE, Tiessler-Sala L, Maréchal JD, Cardona GW (2020) Investigating potential inhibitory effect of *Uncaria tomentosa* (cat's claw) against the main protease 3CL(pro) of SARS-CoV-2 by molecular modeling. *Evid Based Complement Alternat Med* **2020**, 4932572.

31. Boonyasuppayakorn S, Suroengrit A, Srivarangkul P, Yuttithamnon W, Pankaew S, Saelee T, Prompetchara E, Salakij S, et al (2016) Simplified dengue virus microwell plaque assay using an automated quantification program. *J Virol Methods* **237**, 25–31.

32. Wermuth CG, Ganellin CR, Lindberg P, Mitscher LA (1998) Glossary of terms used in medicinal chemistry (IUPAC recommendations 1998). *Pure Appl Chem* **70**, 1129–1143.

33. Opo FADM, Rahman MM, Ahammad F, Ahmed I, Bhuiyan MA, Asiri AM (2021) Structure based pharmacophore modeling, virtual screening, molecular docking and ADMET approaches for identification of natural anti-cancer agents targeting XIAP protein. *Sci Rep* **11**, 4049.

34. Jones G, Willett P, Glen RC, Leach AR, Taylor R (1997) Development and validation of a genetic algorithm for flexible docking. *J Mol Biol* **267**, 727–748.

35. Jetsadawisut W, Nutho B, Meeprasert A, Rungrotmongkol T, Kungwan N, Wolschann P, Hannongbua S (2016) Susceptibility of inhibitors against 3C protease of coxsackievirus A16 and enterovirus A71 causing hand, foot and mouth disease: A molecular dynamics study. *Biophys Chem* **219**, 9–16.

36. Wang J, Su H, Zhang T, Du J, Cui S, Yang F, Jin Q (2014) Inhibition of enterovirus 71 replication by 7-hydroxyflavone and diisopropyl-flavon7-yl phosphate. *PLoS One* **9**, e92565.

37. Yao C, Xi C, Hu K, Gao W, Cai X, Qin J, Lv S, Du C, et al (2018) Inhibition of enterovirus 71 replication and viral 3C protease by quercetin. *Virol J* **15**, 116.

38. Wang J, Zhang T, Du J, Cui S, Yang F, Jin Q (2014) Anti-enterovirus 71 effects of chrysin and its phosphate ester. *PLoS One* **9**, e89668.

39. Zhang W, Qiao H, Lv Y, Wang J, Chen X, Hou Y, Tan R, Li E (2014) Apigenin inhibits enterovirus-71 infection by disrupting viral RNA association with trans-acting factors. *PLoS One* **9**, e110429.

40. Yao C, Xi C, Hu K, Gao W, Cai X, Qin J, Lv S, Du C, et al (2018) Inhibition of enterovirus 71 replication and viral 3C protease by quercetin. *Virol J* **15**, 116.

41. Song JM, Lee KH, Seong BL (2005) Antiviral effect of catechins in green tea on influenza virus. *Antiviral Res* **68**, 66–74.

42. Huan C, Xu W, Ni B, Guo T, Pan H, Jiang L, Li L, Yao J, et al (2021) Epigallocatechin-3-gallate, the main polyphenol in green tea, inhibits porcine epidemic diarrhea virus *in vitro*. *Front Pharmacol* **12**, 628526.

43. Carneiro BM, Batista MN, Braga ACS, Nogueira ML, Rahal P (2016) The green tea molecule EGCG inhibits Zika virus entry. *Virology* **496**, 215–218.

44. Boisnic S, Branchet M-C, Quioc-Salomon B, Doan J, Delva C, Gendron C (2023) Anti-inflammatory and antioxidant effects of diosmetin-3-*O*-β-d-glucuronide, the main metabolite of diosmin: Evidence from *ex vivo* human skin models. *Molecules* **28**, 5591.

45. Mokra D, Joskova M, Mokry J (2022) Therapeutic effects of green tea polyphenol (–)-epigallocatechin-3-gallate (EGCG) in relation to molecular pathways controlling inflammation, oxidative stress, and apoptosis. *Int J Mol Sci* **24**, 340.

Appendix A. Supplementary data

Table S1 List of hit compounds, including their pharmacophore fit scores and GOLD fitness scores with the 3Cpro of EV-A71 and CV-A16.

Compound	Structure	Pharmacophore fit score		GOLD fitness score	
		EV-A71	CV-A16	EV-A71	CV-A16
EGCG		47.6	47.7	60.6	60.5
Diosmin		47.7	47.9	69.3	64.0
RTH-011		47.0	47.4	56.2	53.9
RTH-010		–	45.5	–	–
RTH-012		–	45.5	–	–

Table S2 The cytotoxicity, inhibitory activity, and selective index of diosmin and EGCG toward RD cell infection caused by EV-A71 and CV-A16.

Compound	CC_{50}	EV-A71		CV-A16	
		EC_{50}	SI	EC_{50}	SI
Diosmin	>500 µM	21.02 ± 1.57 µM	23.80	30.68 ± 3.25 µM	16.30
EGCG	>100 µM	12.86 ± 1.30 µM	7.78	15.54 ± 1.50 µM	6.44
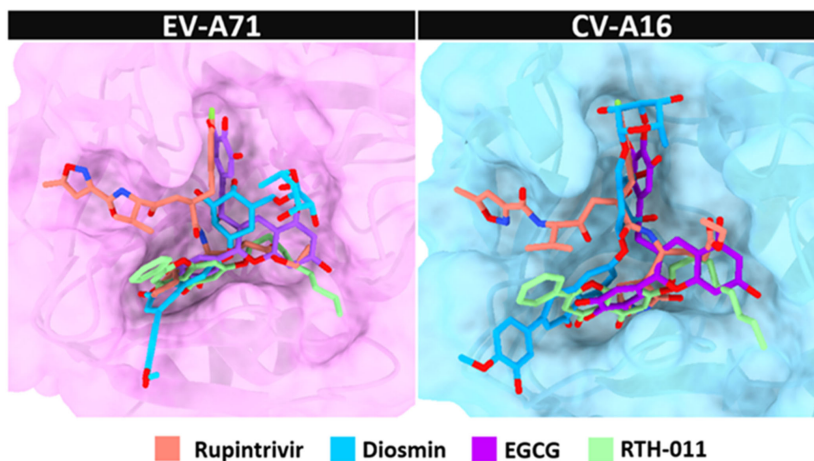
Fig. S1 Binding of the three screened flavonoids within the 3Cpro active sites of EV-A71 and CV-A16, structurally compared with rupintrivir using available crystal structures (PDB IDs: 3R0F and 3SJI).